frontiers | Frontiers in Earth Science

TYPE Original Research
PUBLISHED 10 June 2025
DOI 10.3389/feart.2025.1535083

Check for updates

OPEN ACCESS

EDITED BY
Gilda Maria Currenti,
National Institute of Geophysics and Volcanology (INGV), Italy

REVIEWED BY
Vyacheslav M. Zobin,
University of Colima, Mexico
Yan Zhan,
The Chinese University of Hong Kong, China

*CORRESPONDENCE
Yuyu Li,
yuyuli3@illinois.edu

RECEIVED 26 November 2024
ACCEPTED 07 April 2025
PUBLISHED 10 June 2025

CITATION
Li Y, Gregg PM, Lu Z and Wang J (2025) Stealthy magma system behavior at Veniaminof Volcano, Alaska. *Front. Earth Sci.* 13:1535083. doi: 10.3389/feart.2025.1535083

Stealthy magma system behavior at Veniaminof Volcano, Alaska

Yuyu Li[1]*, Patricia M. Gregg[1], Zhong Lu[2] and Jiahui Wang[2]

[1]Department of Earth Science and Environmental Change, University of Illinois Urbana Champaign, Urbana, IL, United States, [2]Department of Earth Sciences, Southern Methodist University, Dallas, TX, United States

Although Veniaminof Volcano in Alaska experiences frequent eruptions and has eight permanent seismic stations, only two of the past 13 eruptions have had precursory signals that prompted a pre-eruption warning from the Alaska Volcano Observatory (AVO) since 1993. Seismic data from Venianimof indicate that most eruptions from 2000 to 2018 do not coincide with increased seismicity. Additionally, analyses of InSAR data available from 2015 to 2018 which covers the pre-, syn-, and post-eruption periods of the 2018 eruption do not show clear signs of deformation. The systemic lack of systematic precursory signals raises critical questions about why some volcanoes do not exhibit clear unrest prior to eruption. Volcanoes that erupt frequently without precursory signals are often classified as "open" systems with magma migrating through an open network to eruption, rather than pausing at a shallow reservoir. However, the precursory signals, or lack thereof, from a small or deep closed magma system may be difficult to observe, resulting in a stealthy eruption mimicking the behavior of an open system. In this study, we utilize finite element, fluid injection models to investigate a hypothetical closed magma system at Veniaminof and evaluate its ability to erupt with no observable early-warning signals. Specifically, a series of numerical experiments are conducted to determine what model configurations lead to stealthy eruptions – i.e., producing ground deformation below the detection threshold for InSAR (<10 mm) and developing no seismicity, yet resulting in tensile failure which will promote diking and eruption. Model results indicate that the primary control on whether eruption precursors from deformation and seismicity will be present are the rheology of the host rock and the magma flux, followed by the secondary control of the size of the magma chamber, and then its depth and shape. Volcanoes with long-lived thermally mature magma systems with moderate to small magma reservoirs are the most likely to exhibit stealthy behavior, with the smallest systems most likely to fail without producing a deformation signal. This result is likely because small, deep magma systems produce minimal surface deformation and seismicity. For stealthy volcanoes like Veniaminof and others in Alaska (e.g., Cleveland, Shishaldin, Pavlof) and around the world, understanding the underlying magma system dynamics and their potential open vs. closed nature through numerical modeling is critical for providing robust forecasts of future eruptive activity.

KEYWORDS

Aleutian volcanoes, Veniaminof, eruption, volcano forcasting, magma system, finite element model, rheology

1 Introduction

Volcano monitoring and forecasts are crucial to evaluate and mitigate the potential risks and socioeconomic impacts of volcanic activity. Seismicity, ground deformation, and gas emissions are commonly used as precursory signals and play a critical role in providing early warning of volcanic activity and impending eruption (e.g., Segall, 2013; Voight et al., 1998). However, sometimes observations of deformation and/or increase in seismic activity do not correlate with the timing of eruptions (Biggs et al., 2014; Roman and Cashman, 2018). Evaluating volcanoes that lack eruption forecasting signals is necessary to understand the characteristics of stealthy magma systems and develop strategies to mitigate their impacts. Veniaminof, an active caldera system on the central Aleutian Arc of Alaska, exhibits the characteristics of these stealthy eruptions (Figure 1). Although Veniaminof experiences frequent eruptions and currently has eight permanent seismic stations, only two of the past 13 eruptions since 1993 have had precursory phases that prompted a pre-eruption warning from the Alaska Volcano Observatory (AVO; Cameron et al., 2018). Previous research has indicated several hypotheses for why a volcano may erupt without warning, including: magma reservoirs that are too deep to create detectable inflation signals during magma recharge and the migration of eruptive products from a deep mid-crustal reservoir that only transit through the shallow magma storage systems (Grapenthin et al., 2013); magma flux that is below the detectible level; and open volcanic systems that have open vents and frequent degassing resulting in a lack of detectable pre-eruptive ground uplift precursors (Chaussard et al., 2013; Biggs et al., 2014). However, the spectrum between open-vent and closed-system unrest is likely not dichotomous but rather relative, with volcanoes experiencing variations between open and closed modes of unrest (Rose et al., 2013; Acocella et al., 2023). Well-recognized open-vent volcanoes such as Villarrica (Chile), Stromboli (Italy), and Galeras (Colombia) may represent archetypal cases. In contrast, Veniaminof may occupy a position that incorporates elements of both models. The precursory signals from a small or deep closed magma system may be difficult or impossible to distinguish from open vent unrest, as both result in eruptions without observable precursors.

The goal of this study is to investigate the magmatic processes in closed systems that lead to stealthy eruptive behavior characterized by the absence of seismicity (i.e., shear failure) and observable ground deformation, while still resulting in tensile failure leading to dike initiation and eruption. In other words, we aim to investigate how a closed magma system may behave in a way that mimics open system unrest. We use seismicity and ground deformation observations from Veniaminof in conjunction with finite element method (FEM) modeling (Le Mével et al., 2016; Gregg et al., 2012) to address specific questions regarding volcanic activity that does not produce precursory signals of an imminent eruption: 1) What magma system parameters have the greatest effect on observable eruption precursory signals? 2) What parameters are necessary to trigger stealthy eruptions from closed magma systems? 3) What do these findings indicate about the magma system at Veniaminof–such as the associated inter-eruptive behavior, the stability of the system, and its potential for eruption? Axisymmetric, 2D fluid injection models are utilized to identify the configurations that produce ground deformation signals below the detection threshold of InSAR (<10 mm) and no seismicity, while requiring a minimum magma flux needed to produce tensile failure and drive eruption. Elastic models with non-temperature-dependent and temperature-dependent rheology are applied to Veniaminof Volcano to evaluate the overall effect on observation of seismicity and ground deformation. To constrain the cases that result in stealthy eruptions, ones that occur without visible precursory signals, our particular focus is the effects of parameters such as the size, geometry, depth of the magma chamber, and the flux of magma injecting into the conduit and chamber, on the displacement, tensile rupture, and Mohr-Coulomb failure related to the observable precursor signals of InSAR deformation and seismicity.

2 Geologic background

Mt. Veniaminof is an ice-clad, basalt-to-dacite stratovolcano located on the Alaska Peninsula, ~750 km southwest of Anchorage (Figure 1). It is one of the largest caldera-forming volcanoes of the Aleutian arc and is comprised of a 10 km diameter caldera surrounded by 600 m wall scarps formed during caldera-forming eruptions 3.7 kya with an estimated volume of ~350 km^3 (Miller et al., 1998; Bacon et al., 2007). Veniaminof is one of the most active volcanoes in the Aleutians and has erupted at least 15 times in the past 200 years from the intra-caldera cone (~300 m in height). Eruption compositions are primarily basaltic to basaltic andesite, resulting in the formation of minor tephra deposits and small lava volume effusive flows mostly within the boundaries of the caldera (Loewen et al., 2021). Veniaminof is surrounded by extensive pyroclastic-flow deposits from two Holocene caldera-forming eruptions, nine kya and 3.7 kya, and lahar deposits (Miller and Smith, 1987; Bacon et al., 2007). Historical eruptions have produced small-volume basaltic to andesitic deposits from an intra-caldera cone, while the post-3.7 kya dacitic pumice-fall deposit represents explosive silicic eruptions (Fournier and Freymueller, 2008; Bacon et al., 2007). Previous work indicates that the subsurface magma system of Veniaminof consists of a shallow reservoir comprised of a region of segregated felsic magma on top of a crystal mush column where basaltic magmas occasionally intruded (Bacon et al., 2007). The observation of anhydrous phenocryst assemblages and whole-rock geochemistry indicates a dry, reduced, and high-temperature magmatic system (Miller and Smith, 1987).

Since the 1830–1840s, 19 eruptions have been documented (Waythomas et al., 2022), with most occurring without clear early warning, such as the 2004, 2005, 2006, and 2008 eruptions, which were classified as "detect only" by the Alaska Volcano Observatory (Cameron et al., 2018). The most recent eruptions in 2021 and 2018 also lacked distinct precursory signals. The 2021 eruption (VEI 1) was not detected until 3 days after its onset, when sulfur dioxide emissions were observed, followed by increased surface temperatures, an ash cloud, and an ash plume from Cone A, which consisted of small explosions and minimal lava effusion within the glacial melt pit 1 km east of Cone A (Waythomas, 2021; Smithsonian Institution Global Volcanism Program, 2021; Orr et al., 2024). While the 2021 eruption has

10.3389/feart.2025.1535083

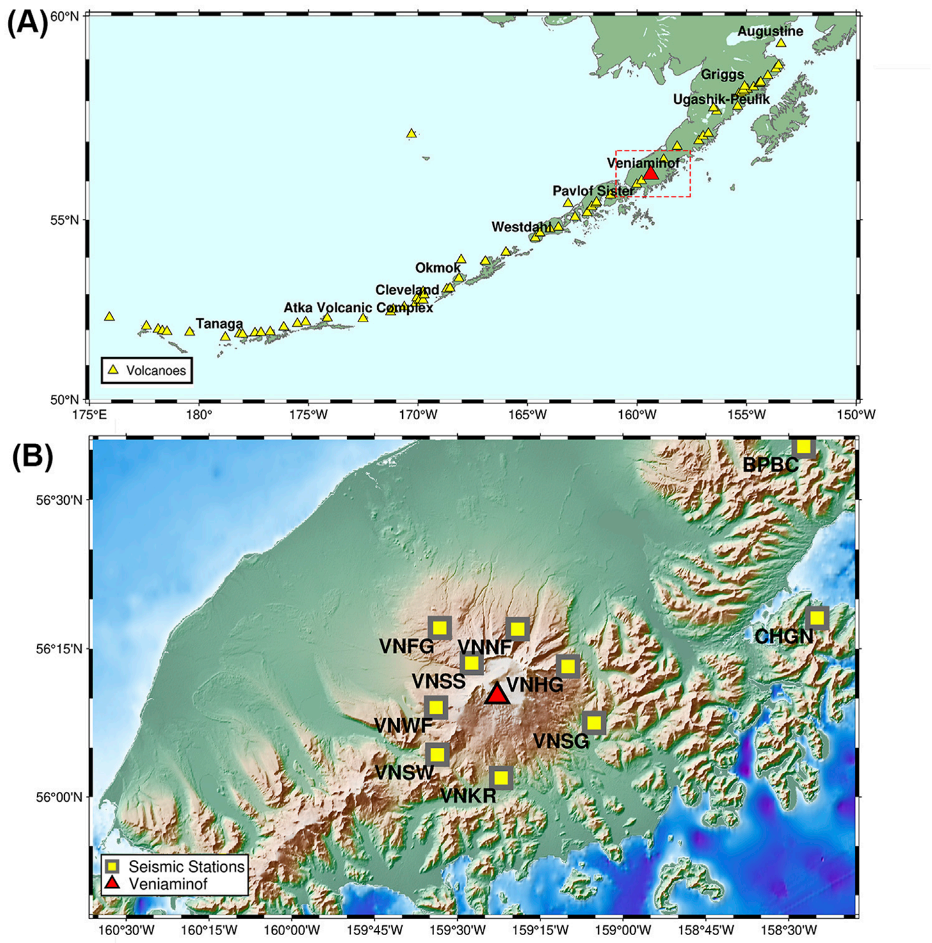

FIGURE 1
Veniaminof Volcano located in the Aleutian Arc, Alaska. **(A)** Coastline map of the volcanoes of Aleutian Arc. Red box represents the location of **(B)**. **(B)** Topographic map of Mt. Veniaminof showing its summit (red triangle) and the locations of eight permanent seismic stations maintained by AVO (yellow squares).

not been analyzed in detail, recent investigations of the 2018 eruption provide insights into the magma system. In fall of 2018, a relatively long-duration eruptive event occurred (VEI 2), lasting from September 4th to December 27th 2018. The strombolian eruption generated a lava flow 800 m long, and minor ash emissions (Smithsonian Institution Global Volcanism Program, 2021). From September to December, the explosivity of the eruption increased producing a continuous ash plume of 400 km on November 21st (Loewen et al., 2021). In addition to the observation from the local seismic networks and satellite images, tephra and lava flow samples have been collected (Wallace et al., 2020; Loewen et al., 2021). Preliminary analyses, including glass geochemistry and whole-rock studies, indicate basaltic andesite products initiating from ~16 km depth with consistent compositions throughout the eruption period (Loewen et al., 2021). While 2018 eruption exhibited low-level volcanic tremor, slight surface temperature increases, and minor steam emissions immediately before its onset, these signals resembled past non-eruptive unrest and occurred too close to onset for reliable warnfing (Waythomas et al., 2022).

Changes in seismicity rate can be a precursory signal of imminent eruption. However, Veniaminof eruptions during 2000–2021 either mismatch changes in cumulative seismicity or have no concurrence with rapid increases in seismicity (Figure 2; Power et al., 2019). Additionally, several increases in seismicity occurred between 2008 and 2013 and no eruptions occurred during this 5-year period. Changes in the cumulative seismicity may correspond with eruptions in 2004, 2008, and 2015, but there is a dearth of shallow earthquakes. Overall, the number of the shallow earthquakes associated with volcanic unrest/eruption at Veniaminof is minimal. These observations indicate that seismicity is not a reliable precursory signal for Veniaminof eruptions, leading to the question of whether Veniaminof is an open system (e.g., Chaussard et al., 2013) or a closed, stealthy magmatic system. To determine the dynamics underlying Veniaminof's

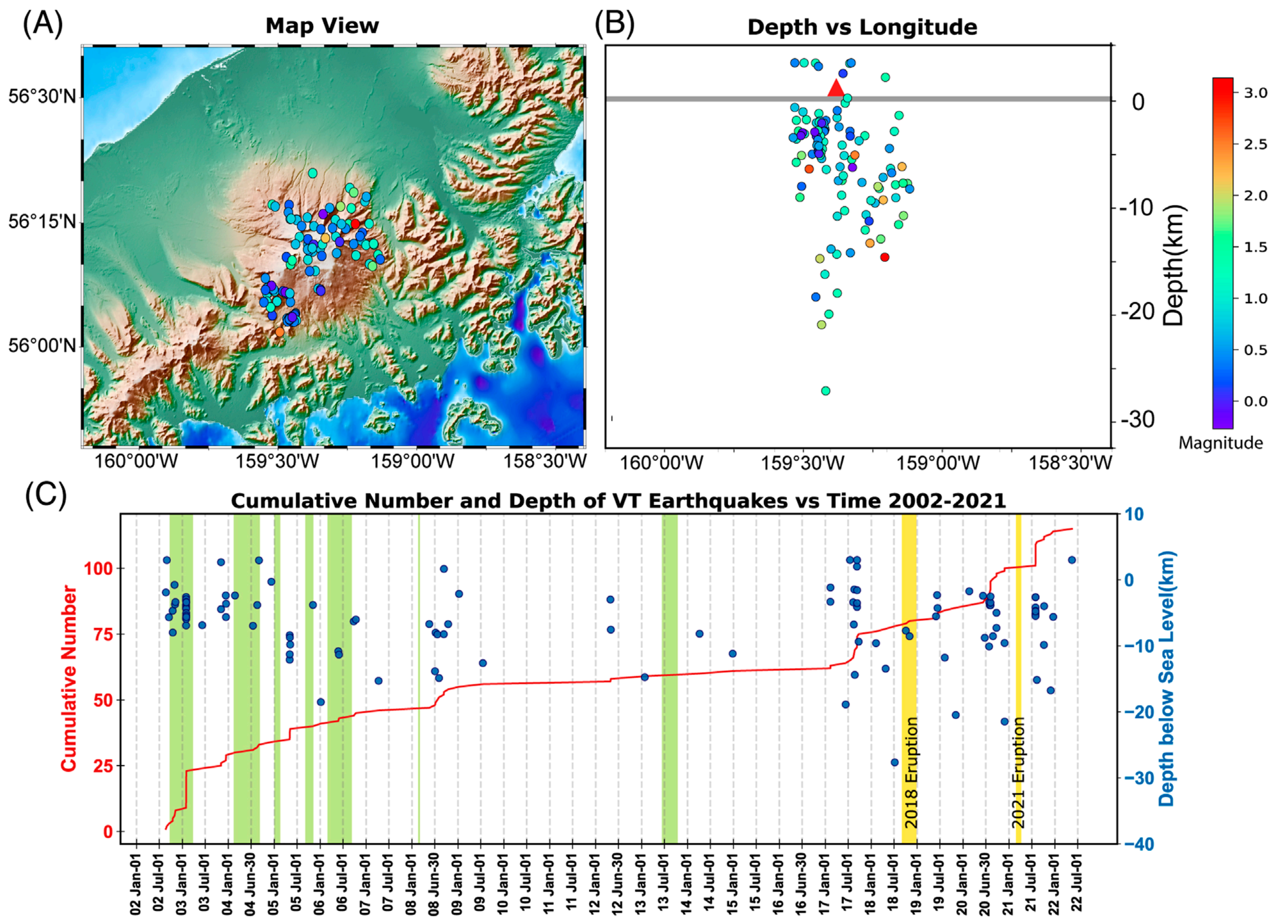

FIGURE 2
Earthquake hypocenters from 2000 to 2021 near Veniaminof Volcano, Alaska. **(A)** Earthquake epicenters within 20 km of the summit color coded by magnitude. **(B)** Longitude *versus* hypcentral depth. The red triangle indicates the location of the Veniaminof summit. **(C)** Hypocentral depth *versus* time and cumulative number of located earthquakes (red line). Green regions indicate eruptive periods. Most eruptions between 2000 and 2021 are not proceeded by increased earthquake activity, while no eruptions between 2008 and 2021 occurred when several increases in earthquake activity were detected. (Power et al., 2019 and personal communication from Power, J.).

activity additional characteristics of its magma reservoir must be examined.

3 Methods

3.1 Persistent Scatter SAR interferometry (PS-InSAR)

To observe the spatiotemporal evolution of the ground deformation before and throughout the 2018 Veniaminof eruption (September to December 2018), Persistent Scatter SAR Interferometry (PS-InSAR) (Ferretti et al., 2000) was applied on the Sentinel-1 data from 2015 to 2018. The summer data (June to October) are selected for each year to obtain the best coherence between images, as the images are impacted by the ice and snow coverage at the caldera of Veniaminof. The SAR images are C-band (wavelength = ~5.56 cm) Single-Look-Complex (SLC) Level 1 products of Sentinel-1A from ascending tracks, using IW swath mode with VV polarization and incidence angle 20°–46°.

StaMPS was used to perform time-series analysis of the SAR acquisitions (Hooper et al., 2004; Hooper, 2006; Hooper et al., 2007; Hooper et al., 2007; Hooper, 2008). The topographic phase was removed from the interferograms with Shuttle Radar Topography Mission (SRTM) one arc-sec (30 m) data. Orbit error and atmospheric phases were estimated and subtracted from differential interferograms during the StaMPS processing.

3.2 Finite element methods

To investigate host rock stability in response to the ground deformation caused by inflation of magma chamber, we use a thermomechanical Finite Element Method (FEM) modeling approach. We build upon previous numerical experiments (Gregg et al., 2012; Grosfils et al., 2015; Le Mével et al., 2016; Gregg et al., 2018) utilizing COMSOL Multiphysics 6.0 to model an inflating magma reservoir at Veniaminof Volcano (Figure 3). The COMSOL modules utilized in this investigation include Heat Transfer Module, Fluid Transfer Module, Nonlinear Materials

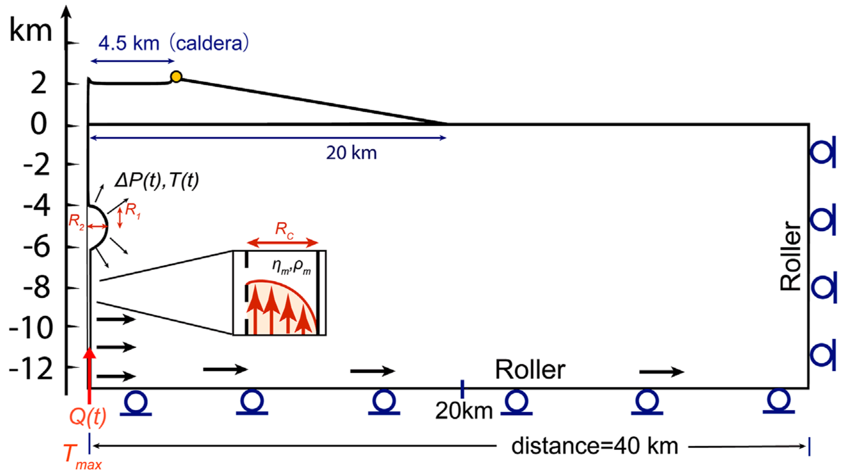

FIGURE 3
Finite element method (FEM) model set up for Veniaminof. The fluid injection approach of Le Mével et al. (2016) is modified to investigate the magma system at Veniaminof and its ability to erupt with no geophysical precursors. An axisymmetric 2D model is set up with side and bottom roller boundaries and the free boundary on surface, including the approximate topography of Veniaminof volcano. Magma intrudes upward from a deep-seated source (>13 km) via a conduit into a shallow reservoir. Volumetric growth of the magma chamber is caused by the magma injection. All the following displacement results (Figures 5–7) are taken as the edge of the caldera (yellow dot in this figure).

Module, and Structure Mechanics Module. The fluid-structure interaction, time-dependent model was constructed following the setup of Le Mével et al. (2016), to solve for temperature, mass transport, and stress and strain in response to magma flux into a shallow reservoir (see Supplementary Tables 1, 2 for a list of parameters and variables). Outputs from the numerical experiments provide constraints on the failure behavior of the host rock surrounding a reservoir.

The 40 by 16 km two-dimensional model space is constructed with a symmetrical central axis, roller boundary conditions are implemented along the side and bottom, and the ground surface is free boundary including an approximate topography of the edifice and caldera of Veniaminof (Figure 3). An existing magma reservoir is assumed with a connecting conduit to accommodate magma transporting from a deeper source (>13 km). The initial magma reservoir is varied in size from 1–6, with Size one being the largest volume and Size six being the smallest, and shape (spherical, oblate, and prolate ellipsoids). The surrounding host rock is modeled as a linear elastic material. For additional details of the model implementation please see the Supplemental Methods.

4 Results

4.1 InSAR-derived ground deformation

The time series of observed ground deformation from summer 2015 to 2018 (before and during 2018 eruption) covering the area of volcano edifice of Veniaminof generated by PS-InSAR are provided in Figure 4. The line of sight (LOS) displacements are in the range of ±3 cm including motion towards the satellite (uplift) and away from the satellite (subsidence). The time series deformation results at each coherent pixel were presented in Supplementary Figure A.1. The uplift and subsidence of a deforming volcano are considered to be the result of the movements of subsurface magma related to the unrest and eruption activities (Dzurisin, 2003). However, the time series of SAR images shows no clear trend. Although our data processing involves the removal of SAR images with high noise, the displacement signals are still ambiguous, and suggest the signals observed in these images are likely due to the atmospheric effects. This lack of an observable volcanic ground deformation signal may indicate that the inflation signal caused by volcanic activity is being masked by the atmospheric effects and below the detection threshold. The detection threshold depends on number of SAR images (more images generate less uncertainty), the atmosphere conditions and topography of the study area, and the algorithms of InSAR approaches (Hanssen, 2001). In the case of Veniaminof, 1–2 cm is the approximate uncertainty of displacement. That is to say, if the precursory signal of inflation prior to the 2018 eruption is below this threshold, a clear trend may not be visible in the time series. Additionally, ground deformation at Veniaminof may be masked by the glacier located in the center of Veniaminof's caldera. In this study we seek to link observations of ground deformation based on the ongoing InSAR data with seismicity to evaluate the stealthy nature of Veniaminof to determine the nature of its magma system that is evolving below the threshold of seismic or ground deformation to be observed as eruptive precursors.

4.2 Sensitivity tests in FEM-Based simulations

The primary goal of our numerical experiments is to determine the model configurations needed to produce stealthy eruptions - in other words, magma system states that produce a ground deformation signal that remains below the detection threshold for InSAR and results in little to no seismicity (as calculated by shear failure throughout the model space) while maintaining a minimum

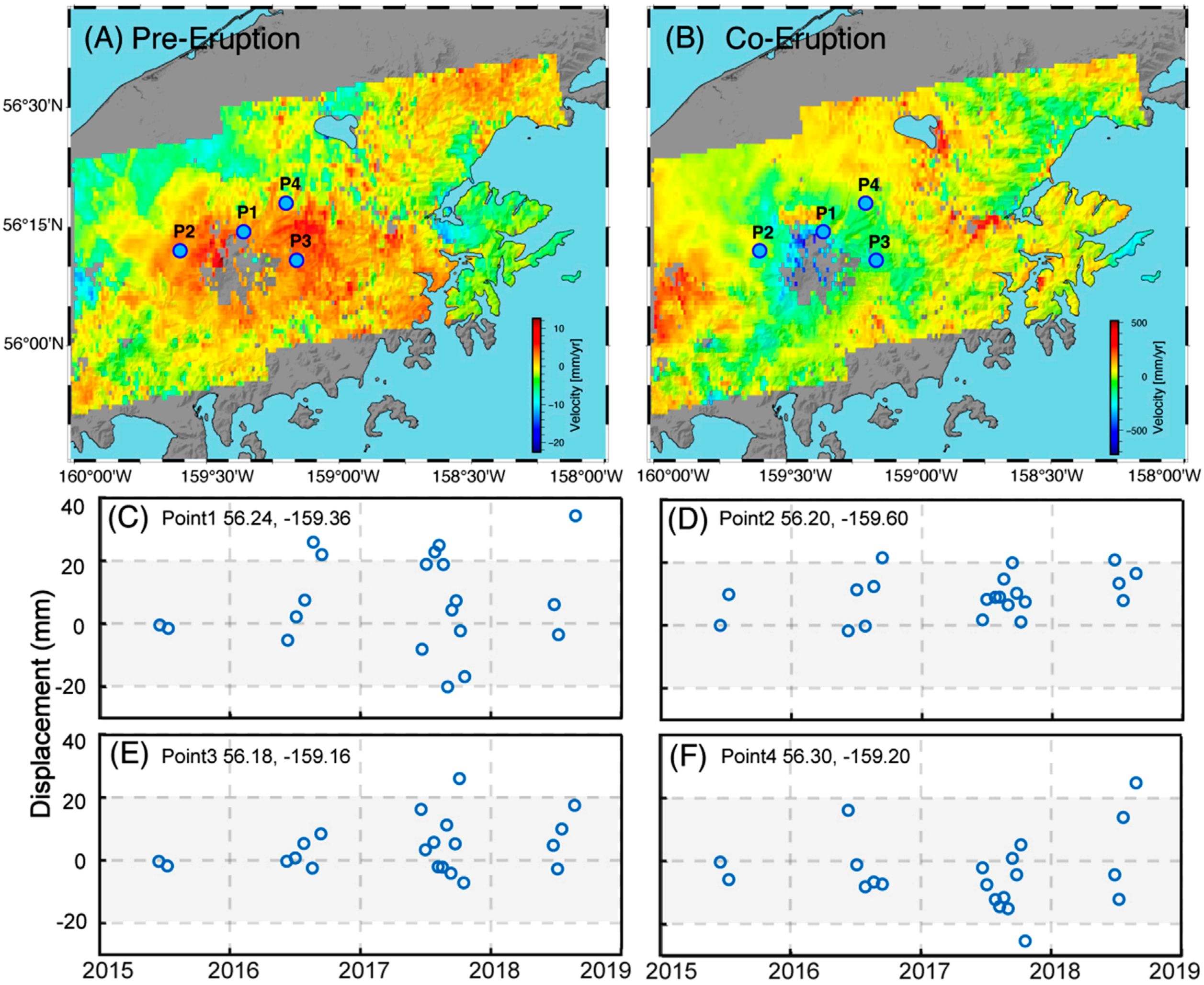

FIGURE 4
Ground deformation and velocity from InSAR time series from 2015 to 2018. **(A,B)** are pre-eruption (June 2015 to August 2018) and co-eruption (September 2018 to October 2018) ground velocity maps generated by PS-InSAR. P1 to P4 are selected locations from near edge to away from edge. The time series of ground deformation of these points are plotted in **(C-F)**. Time series of the ground displacement **(C-F)** for four locations at P1, P2, P3, and P4, respectively.

flux of magma needed to produce the eruptive volume recorded for the 2018 eruption of Veniaminof Volcano. As with other active systems (e.g., Katla and Grímsvötn in Iceland; subglacial volcanoes in Antarctica; Mount Spurr and Westdahl in Alaska) the center portion of Veniaminof is masked from deformation observations due to summit glacier/snow. As such, modeled deformation results are taken from the caldera rim coinciding with where the InSAR observations are coherent.

The numerical results illustrate how observable ground deformation and the stability of magma system are controlled by the underlying magma reservoir characteristics including size, shape, depth, and magma flux (Figures 5–7). First, as is to be expected, shallower magma chambers are associated with higher displacement (Figure 5). Second, higher displacement is directly associated with larger chamber sizes (e.g., Size 1 and Size 2). However, for the largest reservoirs, there is also a dependence on the specific depth, shape, and flux combination as Size 2 can produce slightly higher flank displacements than Size 1 for non-temperature dependent prolate and spherical models. Third, in most cases, oblate chambers are predisposed to maximal displacement, in contrast to the minimal displacements associated with prolate chambers. Note, the difference between the prolate and oblate geometries may be due to the chosen observation spot on the edge of the caldera rather than the center of the summit. An oblate shape will generate more upward displacement as its elongated horizontal shape extends towards the edge, whereas prolate geometries result in greater deformation in the center. In addition, because the deformation is calculated at the caldera edge, the displacement does not always increase with shallower magma chamber depths (Figure 5). For example, the highest displacement value for oblate reservoirs is from −4 to −6 km (Figures 5A,B). Fourth, as is to be expected, a direct correlation exists between magma flux and displacement, with the flux rate being the most crucial factor controlling ground deformation and the timing of failure (Figures 6, 7). Negative values of displacements

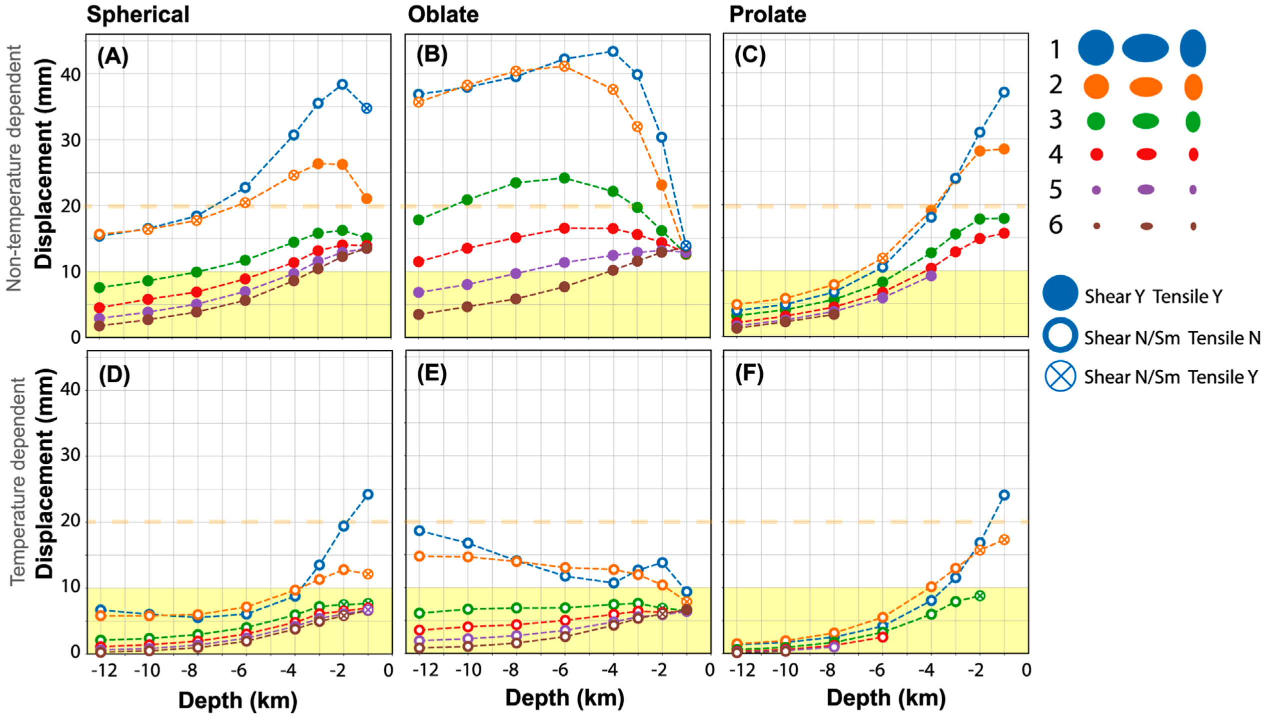

FIGURE 5
Magma chamber depth vs. ground deformation. Depth is to the surface of volcano edifice with summit of ~2 km, while ground deformation is at the edge of summit caldera (see the edge location in Figure 3) caused by inflating magma chamber. Flux is taken assumed to be 0.0507 m^3/s, estimated by the volume of volcanic products produced during the 2018 eruption of Veniaminof. Magma chamber size 1 to 6 (from largest to smallest) represents the scenarios where the eruptible volume of the chamber is 0.16%, 1%, 5%, 10%, 20%, 50% of the overall reservoir volume (see details in Supplementary Table 3). The yellow shaded area indicates displacement from 0 to 10 mm, the detectable threshold of Sentinel one data. The dashed line (20 mm) marks the approximate upper limit of the detectable threshold used in Figure 7. Experiments in **(A-C)** assume a non-temperature dependent models, while **(D-F)** assume a temperature dependent rheology. Y = yes, N = no, Sm = small, Shear = shear failure, and Tensile = tensile failure. "Tensile Y" indicates tensile failure occurred along the reservoir or conduit in the experiment (assuming a tensile strength of 0 MPa as a conservative minimum).

(<0 mm) are generated when the flux rate is <0.01 m^3/s, i.e., 0.0003 km^3/yr. To visualize the relationship, Supplementary Figures A2, A3 provide additional model results for flux values from 0.01 to 0.1 m^3/s with steps of 0.01 m3/s to mimic the case of the flux leading up to Veniaminof's 2018 eruption.

Our study indicates that the key trends apply in both non-temperature dependent and temperature dependent rheological conditions: 1) high flux typically leads to increased displacement and a higher chance of tensile and Mohr-Coulomb failure; 2) shallow depth is associated with high displacement but has very little impact on tensile and Mohr-Coulomb failure; and 3) larger chambers usually exhibit more displacement but are less prone to cause tensile and Coulomb failures.

5 Discussion

5.1 Factors controlling precursory observations

Temperature-dependent models have a lower calculated displacement and, thus, a lower likelihood of producing tensile and shear failure. Therefore, to reach the same displacement and threshold for failure, temperature-dependent models require a higher magma flux rate (Figures 5, 6). Specifically, initiating tensile failure to catalyze eruption requires a higher flux rate than the non-temperature dependent models (i.e., low fluxes of 0.01 m^3/s will not suffice). Figure 7 illustrates different combination of factors and their influence on stealthy eruptions.

1) High flux and large chamber size: high flux combined with a large size tends to produce significant displacement, excluding the likelihood of a stealthy eruption, although Mohr-Coulomb failure may not necessarily be high. This is attributed to the positive association between both high flux and large size with displacement. In temperature-dependent models (Figures 7B,D), a flux of 0.10 m^3/s with large chamber size remains stealthy, and observable eruptions are beyond the plotted range due to the temperature-dependent rheology shifting the upper flux limit for stealthy eruptions rightward.
2) High flux and small chamber size: this combination typically results in high Mohr-Coulomb failure, making seismic signals observable and unambiguous. High flux and small size jointly increase the affected subsurface region of Mohr-Coulomb failure. Yet, this combination contributes to initiate tensile failure, facilitating eruption onset, and displacement may

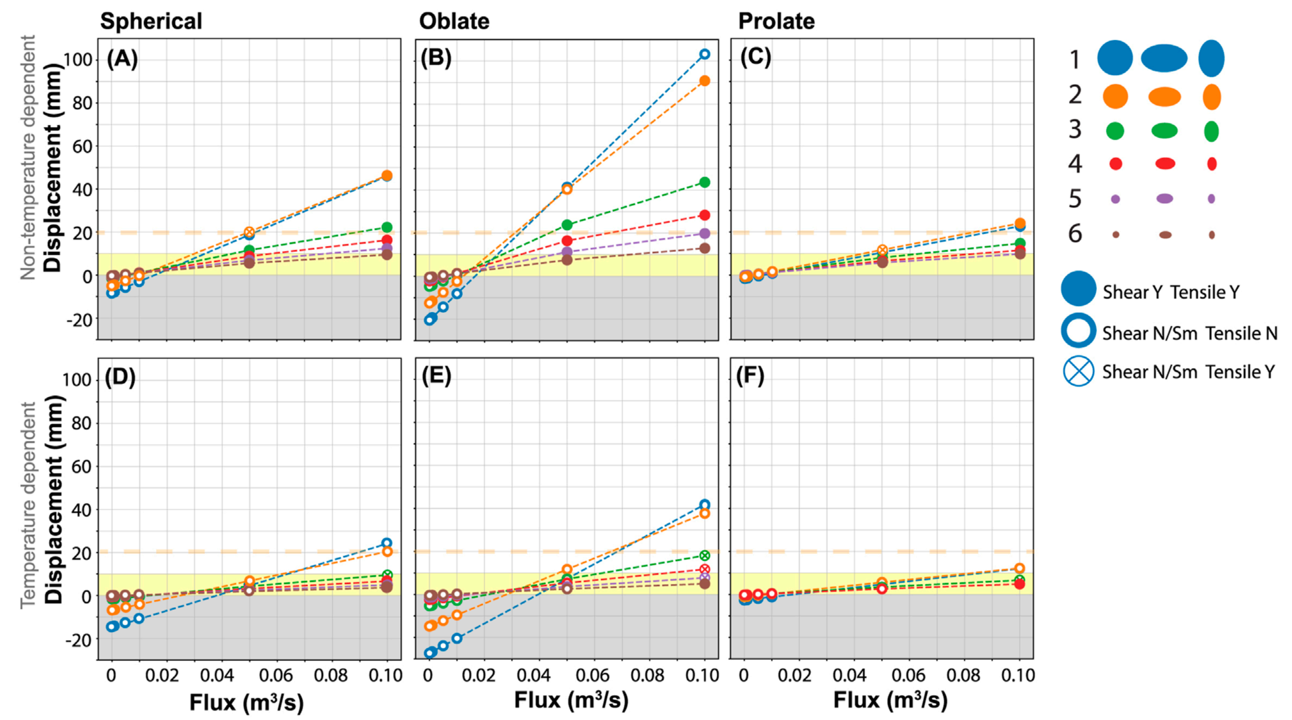

FIGURE 6
Magma flux vs. ground deformation. Ground deformation at the edge of summit caldera caused by inflating magma chamber, with a constant depth = −6 km (depth to the surface of volcano edifice with summit of ~2 km height). Flux = 1e^{-5}, 5e^{-5}, 1e^{-4}, 5e^{-4}, 1e^{-3}, 5e^{-3}, 0.01, 0.05, 0.1 m^3/s. Magma chamber size and shape parameters are described in Supplementary Table 3. The yellow shaded area indicates displacement from 0 to 10 mm, the detectable threshold of Sentinel one data. The dashed line (20 mm) marks the approximate upper limit of the detectable threshold used in Figure 7. The gray shaded region indicates models results of subsidence at the flank. Experiments in **(A-C)** assume a non-temperature dependent models, while **(D-F)** assume a temperature dependent rheology. Y = yes, N = no, Sm = small, Shear = shear failure, and Tensile = tensile failure. "Tensile Y" indicates tensile failure occurred along the reservoir or conduit in the experiment (assuming a tensile strength of 0 MPa as a conservative minimum).

not be significantly high, as the small size counteracts the effect of high flux. This "observable eruption" scenario is illustrated in the unpopulated areas in Figures 7A,C. With temperature dependent rheology (Figures 7B,D), the upper flux limit of "stealthy eruption" shifts rightward, accommodating higher flux values without substantially increasing Mohr-Coulomb failure.

3) Low flux and large chamber size: a low flux coupled with a large chamber size typically prevents tensile failure (i.e., reducing likelihood of triggering of eruption) and Mohr-Coulomb failure, as both low flux and large size decrease the probability of such occurrences, although this might result in low displacement due to low flux. In non-temperature-dependent models, a low flux (0.01–0.02 m^3/s) combined with a large chamber size remains effective, indicating temperature-dependent wall-rock properties amplify the combined effects of low flux and large size, thereby diminishing the likelihood of tensile failure initiation.
4) Low flux and moderate to small chamber size: in this scenario, tensile failure and Mohr-Coulomb failure are unlikely. Although displacement is below the threshold for detection, the absence of tensile failure suggests that an eruption will not occur. While small size increases the likelihood of tensile failure, the predominant influence is the low flux.

Therefore, the primary determinants on eruption precursors from deformation and seismicity are the rheology of the warm wall rock and the magma flux, followed by secondary parameters of the size of the magma chamber, and then its depth and shape. Essentially, a long-lived system with ample thermal input to warm the rheology has a greater parameter space that will produce stealthy eruptions without precursory signals.

Our models, both temperature dependent and non-temperature dependent, are elastic and do not account for the viscosity of the wall rock. A viscoelastic rheology typically results in greater deformation compared to purely elastic models, as the viscous component allows for more prolonged and extensive deformation under stress before reaching failure (Bonafede and Ferrari, 2009; Del Negro et al., 2009; Gregg et al., 2012; Hickey et al., 2013; Newman et al., 2001). However, an elastic model is appropriate when the loading time is shorter than the host rock's relaxation time, and particularly appropriate for Veniaminof which has an inter-eruption time interval of ~5 years which should experience negligible effects due to viscous relaxation (Zhan and Gregg, 2019).

5.1.1 Long-lived vs. transient magma systems: When does temperature matter?

Distinguishing between transient and long-lived magmatic systems is essential for understanding volcanic behavior and

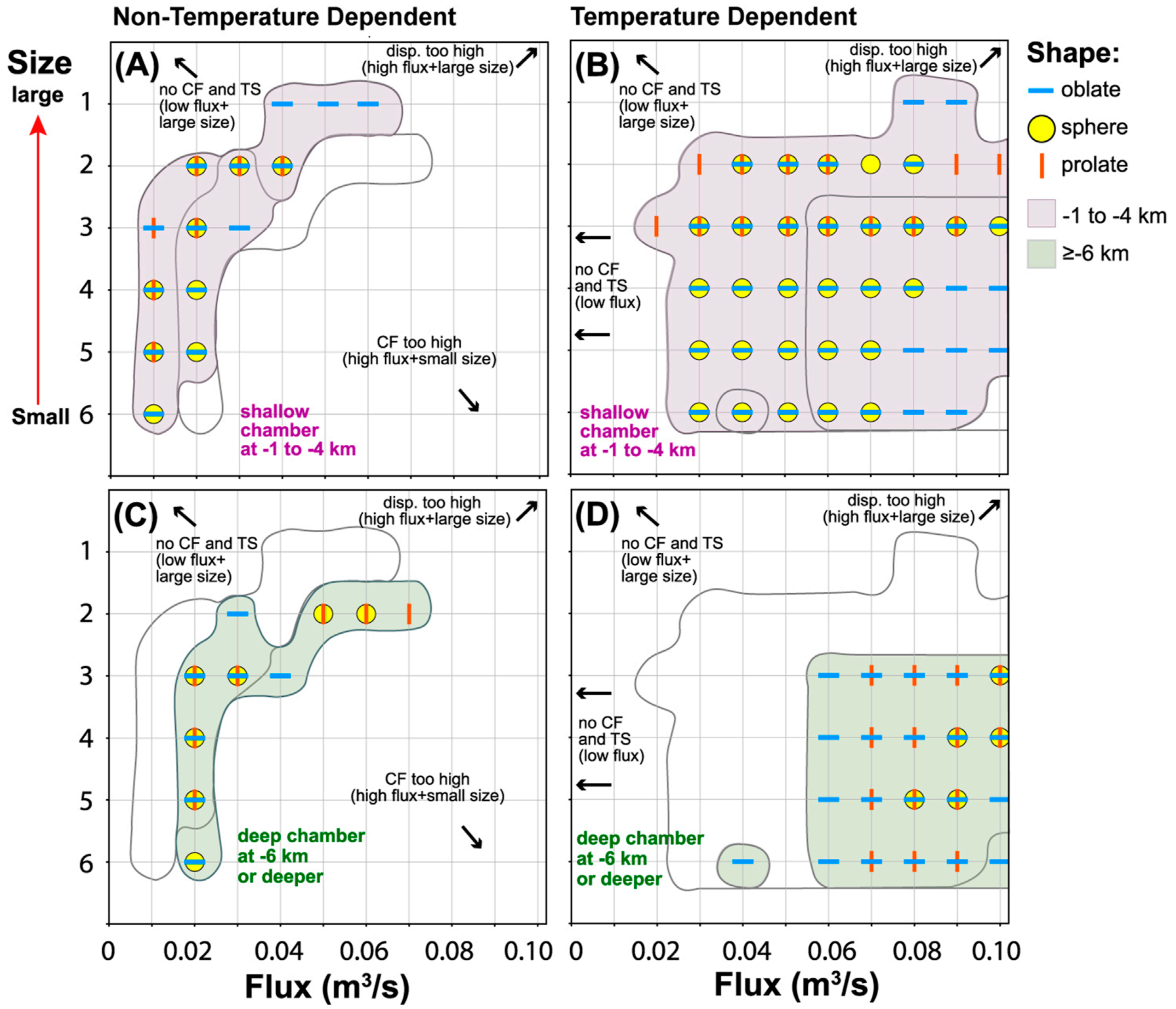

FIGURE 7
The parameter space for stealthy eruptions. Plotted results include models that produce <20 mm of surface displacement and little to no shear failure, but exhibit tensile failure surrounding the magma reservoir. **(A,B)** are the results for shallow magma reservoirs (1–4 km depth below the summit) that produce stealthy eruptions (shaded gray), whereas **(C,D)** illustrate the regions of the parameter space for deeper reservoirs (>6 km depth below the summit) that produce stealthy eruptions (shaded green). The overlap in parameter space is indicated by the black lines for ease of comparison. See Supplementary Table 3 for the specific values of the radius of magma chamber size (1–6) for different shapes. CF = Mohr-Coulomb failure, TS = tensile stress that is over the critical threshold, and disp. = displacement.

associated hazards. Long-lived magma chambers exhibit sustained activity over protracted periods, often with complex, multi-tiered magma chambers, and extend through the crust and comprise heterogeneously distributed melt, crystals, and exsolved volatiles (Cashman et al., 2017). In contrast, transient magmatic systems typically feature ephemeral magma chambers that undergo rapid modifications influenced by processes such as volatile degassing, which critically impact magmatic overpressure and consequently drive volcanic eruptions (Mittal and Richards, 2019). The lifespan of a magma chamber can vary significantly depending on several factors, including the tectonic setting, the composition of the magma, and the dynamics of the magmatic system (Gualda et al., 2012; Cooper et al., 2017; Turner and Costa, 2007), and eruptible portions within long-lived chambers typically last from centuries to hundreds of thousands of years (Karakas et al., 2017).

Veniaminof displays some characteristics of a long-lived system, such as sustained activity over millennia, but the behavior of the 2018 eruption also aligns with aspects of a transient system. Veniaminof's eruption styles vary widely, ranging from effusive to explosive with a history of sustained volcanic activity characteristic of a long-lived system; however, historical eruptions demonstrate simultaneous explosive and effusive activity from separate vents, which could also be indicative of a transient magmatic system (Waythomas, 2021). The eruptive behavior of 2018, evolving in explosivity over time (Loewen et al., 2021; Bennington et al., 2018), might also be consistent with a transient magmatic system.

Moreover, the potentially small magma chamber volume of ~0.8–5 km^3 and relatively low flux rate indicated by our models, as well as the short repose time between its frequent eruptions may suggests a transient magmatic system dynamic. Veniaminof might not maintain a continuous, high level of activity due to a consistent supply of magma, but rather due to more episodic activity, where eruptions occur in response to the accumulation of sufficient magma to initiate failure.

In long-lived magma systems with substantial heat and material influx, the thermal state of the host rock becomes a critical factor for assessing reservoir stability (Gregg et al., 2012; Jellinek and DePaolo, 2003). For example, simulations of magma injection into a long-lived thermally primed host rock indicate that models excluding temperature-dependent elastic moduli and viscosity fail to reproduce realistic stress evolution (Gregg et al., 2018) or observed deformation level (Le Mével et al., 2016). While the inclusion of temperature-dependent rheology is an important factor for estimating the stress evolution when investigating long-lived system dynamics, the non-temperature dependent models might be applicable to Veniaminof given the potentially low flux and a small chamber size estimated by the volume of its volcanic products. The influence of the host rock's thermal state might not be as pronounced when compared to volcanoes with larger, long-lived systems. Nevertheless, including a temperature-dependent host rock in models for Veniaminof may be appropriate. Veniaminof may represent an intermediary scenario within the constraints of parameters tested by our models, embodying a magmatic system that merges aspects of both end-member cases, cold host rock rheology (non-temperature dependent models) and warm host rock rheology (temperature dependent models).

5.2 Stealthy vs. observable magmatic system

Veniaminof Volcano may exemplify a stealthy eruption scenario, confirming that such eruptions are indeed feasible, an eruption characterized by the absence of observable precursory signals including seismicity and ground deformation, but sufficient tensile stress to initiate an eruption without the observable warnings.

5.2.1 Comparison of stealthy and observable closed magma systems

Our models are constructed based on closed volcanic systems and indicate the possibility of two types of eruptions: the "observable" eruption and the "stealthy" eruption. As depicted in Figure 8A, the "observable" eruption encompasses various activity stages. During the pre-eruptive stage, the influx of new magma or the exsolution of volatiles leads to reservoir pressurization and volcanic edifice inflation. This inflation, both in distance and elevation on the surface, can be detected using methods such as InSAR or GPS (Figure 8A1). Additionally, during this stage, the wall rock experiences stress due to magma ejection from the deep source. As a result, rupture of the wall rock occurs around the chamber and conduit region, accompanied by a significant number of volcano-tectonic earthquakes corresponding to shear failure. When the pressure surpasses the crustal strength and the tensile stress on the wall rock exceeds the critical threshold of 0 MPa (chosen as an end-member, minimum value), magma can ascend through a conduit/dike toward the surface, initiating the volcano's eruption (Figure 8; Supplementary Figure A2). Once the eruption commences, during its co-eruptive stage, the removal of magma and gas from the reservoir causes the magma chambers to contract and the pressure to decrease. Consequently, deflation surface signals can be observed, unless there is additional recharge during the eruption. Additionally, in the usual case, volcano-tectonic earthquakes disperse during this stage. During the post-eruptive (cooling) stage, characterized by the deflation of the edifice (Figure 8; Supplementary Figure A3), deflation signals are evident, and there is no further increase in volcano-tectonic earthquakes. Vents or dykes are sealed by solidification and cooling, and solidification and crystallization occur within magma reservoirs. When no magma is supplied from the depth to the shallow magma system, the volcano remains dormant, with no surface deformation or seismic signals observed (Figure 8; Supplementary Figure A4). After a period of dormancy, the cycle recommences.

Ideally, the detection of both earthquakes and ground deformation enables successful forecasts of volcanic eruptions, including detailed predictions of their timing, location, and magnitude. Notable examples include the 1980 eruption of Mount St. Helens, with accurate forecasts of all subsequent eruptions from April 1981 to December 1982 based on seismic and deformation data, leading to precise predictions without false alarms (Malone et al., 1983; Swanson et al., 1983), the 1991 eruption of Mount Pinatubo, where forecasting significantly mitigated hazards and saved thousands of lives (Voight et al., 1998; 1999), and the accurate short-term prediction of the 2000 Hekla eruption (Soosalu et al., 2005), and these cases highlight the importance of integrating seismic, deformation, and other geophysical data for effective eruption forecasting (Segall, 2013). It is worth noting that an unerupted unrest scenario, marked by observable deformation and seismic signals without a subsequent eruption, can arise, e.g., the Westdahl volcano in the Aleutian Islands displayed significant inflation signals, typically considered precursors to eruptions, yet no eruption occurred within the observed timeframes (Lu et al., 2000; Gong et al., 2015).

In contrast, the stealthy eruption presents a starkly different scenario compared to its observable counterpart, characterized by minimal detectable signals. During the pre-eruptive stage of a stealthy eruption (depicted in Figure 8; Supplementary Figure B1), the wall rock is stressed due to magma ejection from deep sources. The accumulation of volcano-tectonic (VT) earthquakes may not be readily apparent because, according to our models, there is only minimal shear failure around the magma chamber, with no shear failure detected around the conduit. While edifice inflation occurs, the signals of Line of Sight (LOS) displacement are too subtle to be detected with current monitoring techniques like InSAR. In such cases, the magma reservoir pressurizes, and the tensile stress exceeds the strength of the surrounding crust, potentially leading to an eruption without observable surface inflation or an increase in seismic activity. In the co-eruptive stage, despite the opening of a dyke or conduit resulting in the release of gas and magma from the reservoir, there remains no detectable ground deflation or significant seismic activity, highlighting the eruption's stealthy nature (Figure 8; Supplementary Figure B2). Similar to observable eruptions, this is followed by the post-eruptive (cooling) stage, where vents collapse

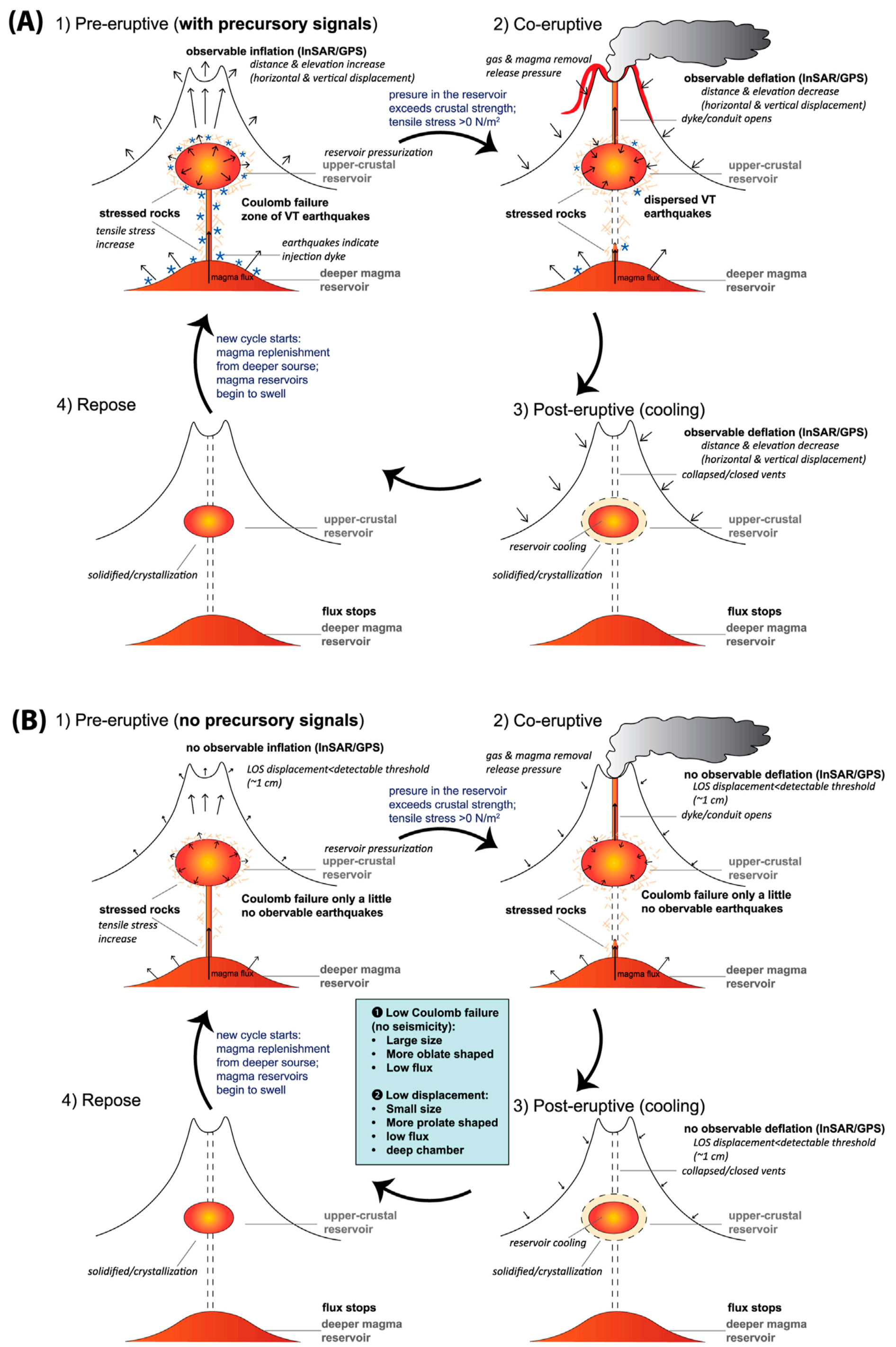

FIGURE 8
Schematic illustration of eruptive cycle model of two cases: **(A)** observable eruption and **(B)** stealthy eruption. The cycle consists of stages 1) pre-eruptive, when shallow magma inflates as it is fed by the deeper source through the conduit, 2) co-eruptive, when eruption starts as tensile stress exceeds the critical threshold (>0N/m^2) and deflation follows as a result of release of magma from chamber, 3) post-eruptive, the cooling stage with deflation of magma chamber, and 4) repose, when flux stopped from deeper magma reservoir and the shallow magma chamber crystallize. In the **(A)** observable eruption case, upward ground deformation due to the inflation of magma chamber can be detected by InSAR/GPS and increase in number of volcano-tectonic earthquakes caused by the Coulomb failure can be observed (stage 1), and deflation ground deformation signal can be detected since the eruption occurs (stage 2). In contrast, in the **(B)** stealthy eruption case, no ground deformation and earthquake precursors can be detected at both pre-eruptive stage (stage 1) and co-eruptive stage (stage 2) because the displacement and Coulomb failure are too low. Inspired by the figure in Chaussard et al. (2013).

or close, and the magma in the upper-crustal reservoir solidifies and crystallizes, cooling the reservoir without observable signals of these processes (Figure 8; Supplementary Figure B3). And finally, the repose stage heralds the onset of a new cycle, with magma replenishment from deeper sources leading to the swelling of magma reservoirs and setting the stage for the next eruption cycle (Figure 8; Supplementary Figure B4).

The stealthy eruption cycle often evades early detection due to its subtle manifestations, posing challenges in monitoring and forecasting with current technological capabilities. The magma system can either be long-lived or transient. To produce stealthy eruptions, a lack of seismicity requires a large reservoir size, more oblate shape, and low flux, while low displacement requires a small reservoir size, more prolate shape, low flux, and a deeper chamber. Considering the host rock rheology, long-lived, thermally primed magma systems allow for a wider range of the parameter space to result in feasible scenarios for stealthy eruption as opposed to transient systems (Figure 7).

5.2.2 Veniaminof: open or closed and stealthy?

Many volcanoes that erupt without observed deformation have long been classified as open-system volcanoes (e.g., Chaussard et al., 2013). In open systems, triggers of eruption include minor magma intrusions, conduit over-pressurization, or lava dome destabilization. One interpretation suggests the deeply rooted plumbing systems pressurize before eruption such as Cleveland and Pavlof volcanoes in Alaska (Lu and Dzurisin, 2014), Galeras in Columbia (Fournier et al., 2010), and Stromboli in Italy, an open-conduit volcano with persistent activity >1,000 years fed by deep seated gas-rich magma (Barberi et al., 2009). Systems with established shallow reservoirs, exhibiting low precursory deformation and the existence of persistent or semi-persistent pathways for magma ascent, are exemplified by volcanoes such as Popocatépetl and Colima in Mexico, and Merapi in Indonesia (Chaussard et al., 2013). Like Veniaminof, the 1999 sub-Plinian basaltic eruption of Shishaldin, Alaska also eluded prediction efforts due to the lack of precursory signals of both InSAR-detectable deformation and VT earthquakes (Lu and Dzurisin, 2014; Moran et al., 2006), although later studies suggested that a swarm of deep long-period (LP) earthquakes, coupled with short-period earthquakes, should have been recognized as precursory signals (Power et al., 2004; Rasmussen et al., 2018). Shishaldin's lack of precursory signals aligns with both closed-system stealthy eruptions and open-system eruptions; yet vapor saturation pressure studies indicate the inclusion compositions are more consistent with open-system degassing, characterized by a predominant release of CO_2 before H_2O (Rasmussen et al., 2018).

Should Veniaminof be considered stealthy, fed by a closed magmatic system? Some geophysical observations (lack of precursory seismicity and observations of ground deformation) and the frequent eruptions at Veniaminof may point to an open volcanic system. According to the volcanic activity summary by AVO (Orr et al., 2024), the majority of historical eruptions since 1830 have likely originated from cone A. This apparent recurrence of eruptions from the same vent could suggest the presence of an open conduit system. Loewen et al. (2021) characterize the 2018 eruption as an exemplar of a frequently active open-vent system, which explains several of Veniaminof's characteristics: nearly continuous, low-level background seismicity punctuated by two periods of elevated tremors linked to increased tachylite textures that indicate the intense ash production and possibly reflecting a deeper conduit to initiate seismic tremors; explosive activity alongside lava flows integrating into the ice cap; and a transition from Strombolian to Hawaiian eruption styles, indicative of varying gas release and magma dynamics. Nonetheless, while seismic tremors and mineral textures indirectly hint at continuous gas emissions, there is no direct evidence of steady outgassing of volcanic gases (SO_2, CO_2, H_2O) through eruptions or even quiescent periods (Rose et al., 2013; Lyons et al., 2011) and a lack of robust documentation on exceptionally high gas emissions (a hallmark of open-vent systems) or detailed studies correlating continuous gas flux with seismic activity during past eruptions. Additionally, the continuous seismic activity indicating magma movement within the volcanic conduit, typical of open-vent volcanism, is not prominent in Veniaminof's history, as shown by the low number of detected shallow VT earthquakes. The presence of a persistent lava lake or exposed fresh lava in the form of a dome with frequent gas emissions common in some open-vent volcanoes (Rose et al., 2013) remains unconfirmed. Furthermore, detailed investigation of variations in seismic velocity structure shows decreases in the seismic velocities prior to Veniaminof's 2004 and 2013 eruptions indicating the potential buildup of magmatic fluids in a closed magmatic system (Bennington et al., 2018). The detailed architecture and dynamics of the magma plumbing system, particularly regarding conduit dynamics essential for sustaining an open-vent paradigm, remain unclear. Detailed analyses of infrasound data to predict open-vent eruptions, used at Villarrica, Chile (Johnson et al., 2018), have yet to be applied to Veniaminof. These gaps complicate classifying Veniaminof's magmatic system and determining how closely it conforms to the open-vent model.

The pattern of eruption frequency at Veniaminof does not strictly align with the open system hypothesis. Its historical explosive eruptions including those recent events in 2013, 1983, and 1956 (up to VEI 3, Global Volcanism Program, 2021), may result from new magma injections into a shallow chamber, similar to Askja, Iceland, Krakatau, Indonesia, Nevado del Ruiz, Colombia, and St. Helens, United States which are characterized as closed systems (Colucci and Papale, 2021). Furthermore, concerning its absence of long-term, edifice-wide ground deformation, often linked to open-vent systems, it is critical to note that InSAR data for Veniaminof excludes the summit caldera due to ice coverage but the periphery area. Our models suggest that scenarios producing 15–18 mm of LOS displacement at the caldera's edge, which falls below Sentinel-1 detection threshold, could indicate 40–270 mm deformation at the center, depending on the chamber's shape, size, depth, and magma flux. Should caldera data become accessible, we might observe ground deformation indicative of stealthy closed-system eruptions (instead of open-vent eruptions), characterized by negligible peripheral deformation and a marginal increase in seismic activity, driven by low magma influx or warm rheology.

5.3 Implications for future monitoring of volcanic systems

Recent technological advancements in data collection and analysis have significantly enhanced our capabilities on volcano monitoring and forecasting. Yet, we are still facing complexities in volcano monitoring and forecasting, including the need for approaches that forecast not only the likelihood of an eruption but also its location, magnitude, style, duration, and potential for ash plumes that impact a long distance (Segall, 2013; Acocella, 2014; Bebbington and Jenkins, 2019). The challenges in short-term volcanic eruption forecasting are significantly heightened by the absence of reliable eruptive precursors despite of the expansion of instrumental networks, the complexity of non-linear pre-eruptive behaviors, and the inherent unpredictability of volcanic systems due to unknown parameters and the potential for sudden changes (Sparks et al., 2012; Acocella, 2014). Specifically, data processing and magma system modeling in forecasting efforts still face significant challenges in quantitatively linking monitoring data to the probabilities of future volcanic events, a limited understanding of volcanic physics, geometries and material properties for physics based modeling, specialization of models for mathematical and computational viability that complicate the task of choosing appropriate models for an as-yet unobserved eruption (Marzocchi and Bebbington, 2012; Poland and Anderson, 2020). Although novel machine learning approaches have facilitated forecasting by detecting critical changes in volcanic activity patterns that indicate transitions at the onset or end of volcanic activity (e.g., classification method by Manley et al., 2021) and despite of advancements in algorithms, the application of machine learning faces challenges including the opaqueness of "black box" models, lack of insights into underlying physical mechanisms, and data limitations due to scarce well-monitored eruptions (Reichstein et al., 2019).

Observable eruptions exhibiting seismicity, deformation, and gas emissions, as depicted in Figure 8A are the subjects of extensive research. As they allow for direct monitoring of precursory signals, there have been successful forecasts of such volcanic eruptions (e.g., Segall, 2013). In cases where eruptions lack detectable precursory seismic activity, alternative indicators such as deformation and increased gas emissions (such as exemplified by Redoubt Volcano) can provide warnings (Roman and Cashman, 2018), and usually average duration of deformation and degassing (932 days and 282 days, respectively) are longer than seismic unrest (197-day) (Phillipson et al., 2013). Additionally, continuous local stress field monitoring, detectable through changes in seismic velocity and shear-wave splitting, may reveal aseismic staging. Meanwhile, small-scale earthquake swarms, indicative of shallow magma chamber recharging, suggest a years-long eruption risk eruption potential. The deep seismic activity may serve as a near-term harbinger of imminent eruption (Roman and Cashman, 2018).

In scenarios where ground deformation remains undetected by GNSS and InSAR despite sufficient coverage of the volcanic edifice, it is important to recognize these techniques' inherent limitations, which have been well documented (Arrowsmith et al., 2021). For example, during the episodes of intense volcanic activity at Mount Etna during spectacular lava fountains, no discernible signals were observed in GNSS or InSAR datasets (Currenti and Bonaccorso, 2019; Carleo et al., 2023; Cardone et al., 2024). These techniques often fail to capture ground deformation induced by small, short-term volcanic events with millimeter- to centimeter-scale accuracy, prompting the deployment of high-precision borehole instruments, such as tiltmeters and strainmeters, on volcano flanks to complement GNSS data and better resolve pre-eruptive deformation (Dzurisin, 2007; Linde and Sacks, 1995; Currenti and Bonaccorso, 2019; Carleo et al., 2023; Cardone et al., 2024). Furthermore, continuing technological research is exploring innovative methods for volcano deformation monitoring, including the fiber optic sensing, which is highly sensitive to external physical processes and observables at specific locations (Jousset et al., 2025).

In addition to ground-deformation techniques, infrasound monitoring can capture signals of volcanic activity that InSAR or GPS fail to detect, as inaudible low-frequency sound waves are generated by processes such as effusive eruptions and lava lake agitation near volcanic vents (Matoza and Fee, 2018). Real-time analysis of these persistent infrasound signals, emblematic of degassing activities within open-vent systems, alongside seismic and gas compositional data, is crucial for providing key insights into degassing styles and persistent degassing pulses for early eruption forecasting, exemplified by the studies on sustained infrasonic tremor observed at volcanoes like Stromboli, Kilauea, Villarrica, and Shishaldin (Johnson et al., 2018). Open-vent volcanoes are also subject to geochemical monitoring of emissions-whether as plumes, fumaroles, through soil diffusion, or via springs (Edmonds, 2021), with measurements like SO_2 emissions being particularly informative (Wilkes et al., 2023; Coppola et al., 2019). Moreover, the characteristic "excess degassing" behavior of open-vent volcanoes, which release more gas than contained in the erupted magma, points to a process of endogenous or cryptic growth magmatic system-the intrusion of unerupted magma within the volcano that does not result in substantial long-term surface deformation. This process is detectable through satellite-derived thermal anomalies in addition to gas emission measurements (Coppola et al., 2019).

5.3.1 Monitoring enhancements at veniaminof volcano

Enhancing future monitoring and forecasting capabilities for Veniaminof Volcano necessitates overcoming significant challenges posed by the existing technological limitations. The high-elevation, steep-slope terrain and snow-covered landscape of Veniaminof present formidable obstacles to detecting volcanic deformation via InSAR, primarily due to atmospheric noise interference and loss of coherence over the volcano summit. Possible strategies to enhance detection accuracy include enhancing InSAR coherence using long-wavelength SARs with much shorter temporal repeats and employing variogram modeling for precise simulation of residual atmospheric noise (Beker et al., 2023). Moreover, supplementing InSAR with campaign GPS systems in the vicinity of the caldera could provide detailed temporal changes in the volcanic system from pre-eruptive stages to inform future eruption predictions (previous campaign GPS at Veniaminof, e.g., Fournier and Freymueller, 2008; Drooff and Freymueller, 2021). Furthermore, deploying high-precision borehole instruments, such as tiltmeters and strainmeters, on volcano flanks could improve the detection of subtle ground deformation (e.g., Currenti and Bonaccorso, 2019; Cardone et al., 2024). Additionally, AVO has been upgrading the Aleutian seismic network to broadband seismometers with real-time digital transmission since 2003, with the upgrade at Veniaminof completed in 2022 (Power et al., 2020). By applying advanced machine learning methods to seismic signal processing, the ability to detect volcanic precursor signals amidst background noise may be greatly improved (Zhu and Beroza, 2018; Malfante et al., 2018; Bueno et al., 2020).

For stealthy volcanoes like Veniaminof and others in Alaska (e.g., Loewen et al., 2021) and around the world, numerical modeling is an invaluable tool. Numerical models of magma reservoir evolution significantly aid in deciphering the processes that lead to the accumulation and transport of magma and eruption-triggering mechanisms, essential for forecasting the future behavior of volcanoes (Caricchi et al., 2021). The 2D FEM models in our study, for example, offer insights into the key factors controlling stress accumulation in the host rock of magma reservoirs including the size, shape depth of the magma chamber, and magma supply rate. Thus, they enhance our understanding of the physical and thermal evolution of volcanic plumbing systems and the conditions that lead to rock rupture and eruption. These are critical for forecasting eruption repose times and guiding strategic data collection efforts.

6 Conclusion

Our comprehensive study on Veniaminof Volcano offers pivotal insights into the behavior and characteristics of "stealthy" volcanic eruptions: characterized by the absence of detectable seismic or geodetic precursors, despite the occurrence of an eruption. The numerical modeling results of Veniaminof Volcano, exemplifying stealthy volcanic eruptions within closed magmatic systems, illuminate key factors necessary for such eruptions that occur with minimal ground deformation and seismicity rate changes, based on a series of constraints on various parameter combinations, including magma chamber size, shape, depth, and magma flux rate, under both temperature-dependent and non-temperature-dependent host rock rheology.

Two critical conditions are a low magma flux rate and a warm rheology of the host rock. A reduced magma ascent rate ensures minimal stress on surrounding rock, limiting ground deformation and volcano-tectonic earthquakes. Warm rheology allows gradual magma movement and deformation within detectable thresholds, generating fewer seismic signals.

Veniaminof's eruptive cycle, including pre-eruptive, co-eruptive, post-eruptive, and repose stages, provides a framework applicable to other volcanic systems globally. Insights from Veniaminof's stealthy eruption guide future forecasts and highlight the need to integrate multidisciplinary data and numerical modeling for accurate predictions. This enhances risk mitigation strategies, reducing volcanic hazards' impact on communities. This study serves as a model for similar volcanoes and advances future monitoring and forecasting efforts in volcanology.

Data availability statement

The original contributions presented in the study are included in the article/Supplementary Material, further inquiries can be directed to the corresponding author.

Author contributions

YL: Conceptualization, Data curation, Formal Analysis, Investigation, Methodology, Validation, Visualization, Writing – original draft, Writing – review and editing. PG: Conceptualization, Funding acquisition, Methodology, Project administration, Supervision, Writing – original draft, Writing – review and editing. ZL: Conceptualization, Funding acquisition, Writing – original draft, Writing – review and editing. JW: Writing – original draft, Writing – review and editing.

Funding

The author(s) declare that financial support was received for the research and/or publication of this article. Investigations of volcanic unrest in the Aleutians is supported by grants from the U.S. National Science Foundation (EAR 1752477, EAR 2122745 – Gregg and Li) and NASA (80-NSSC19K-0357 – Gregg, Wang, and Lu).

Acknowledgments

The authors thank the anonymous reviewers and V. Acocella whose comments and discussions greatly improved the manuscript. We also thank R. Maguire, M. Loewan, M. Head, and C. Lundstrom for helpful discussions that greatly enhanced this investigation.

Conflict of interest

The authors declare that the research was conducted in the absence of any commercial or financial relationships that could be construed as a potential conflict of interest.

Generative AI statement

The author(s) declare that no Generative AI was used in the creation of this manuscript.

Publisher's note

Supplementary material

The Supplementary Material for this article can be found online at: https://www.frontiersin.org/articles/10.3389/feart.2025.1535083/full#supplementary-material

References

Acocella, V. (2014). Great challenges in volcanology: how does the volcano factory work? *Front. Earth Sci.* 2. doi:10.3389/feart.2014.00004

Acocella, V., Ripepe, M., Rivalta, E., Peltier, A., Galetto, F., and Joseph, E. (2023). Towards scientific forecasting of magmatic eruptions. *Nat. Rev. Earth Environ.* 5, 5–22. doi:10.1038/s43017-023-00492-z

Arrowsmith, J. R., Brodsky, E. E., Cooper, C. M., Elliott, J. L., Fee, D., Fischer, K. M., et al. (2021). *Recommendations for enabling earth science through NSF's geophysical facility – a portfolio review of EAR seismology and geodesy instrumentation*. Alexandria, VA, United States: US National Science Foundation.

Bacon, C. R., Sisson, T. W., and Mazdab, F. K. (2007). Young cumulate complex beneath Veniaminof caldera, Aleutian arc, dated by zircon in erupted plutonic blocks. *Geol.* 35, 491. doi:10.1130/G23446A.1

Barberi, F., Civetta, L., Rosi, M., and Scandone, R. (2009). Chronology of the 2007 eruption of Stromboli and the activity of the scientific synthesis group. *J. Volcanol. Geotherm. Res.* 182, 123–130. doi:10.1016/j.jvolgeores.2008.09.019

Bebbington, M. S., and Jenkins, S. F. (2019). Intra-eruption forecasting. *Bull. Volcanol.* 81, 34. doi:10.1007/s00445-019-1294-9

Beker, T., Ansari, H., Montazeri, S., Song, Q., and Zhu, X. X. (2023). Deep learning for subtle volcanic deformation detection with InSAR data in central volcanic zone. *IEEE Trans. Geosci. Remote Sens.* 61, 1–20. doi:10.1109/TGRS.2023.3318469

Bennington, N., Haney, M., Thurber, C., and Zeng, X. (2018). Inferring magma dynamics at Veniaminof Volcano via application of ambient noise. *Geophys. Res. Lett.* 45. doi:10.1029/2018GL079909

Biggs, J., Ebmeier, S. K., Aspinall, W. P., Lu, Z., Pritchard, M. E., Sparks, R. S. J., et al. (2014). Global link between deformation and volcanic eruption quantified by satellite imagery. *Nat. Commun.* 5, 3471. doi:10.1038/ncomms4471

Bonafede, M., and Ferrari, C. (2009). Analytical models of deformation and residual gravity changes due to a Mogi source in a viscoelastic medium. *Tectonophysics* 471, 4–13. doi:10.1016/j.tecto.2008.10.006

Bueno, A., Zuccarello, L., Díaz-Moreno, A., Woollam, J., Titos, M., Benítez, C., et al. (2020). PICOSS: Python interface for the classification of seismic signals. *Comput. and Geosciences* 142, 104531. doi:10.1016/j.cageo.2020.104531

Cameron, C. E., Prejean, S. G., Coombs, M. L., Wallace, K. L., Power, J. A., and Roman, D. C. (2018). Alaska volcano observatory alert and forecasting timeliness: 1989–2017. *Front. Earth Sci.* 6, 86. doi:10.3389/feart.2018.00086

Cardone, M., Cannata, A., Giuffrida, M., Iozzia, A., Minio, V., Viccaro, M., et al. (2024). Changing magma recharge/discharge dynamics during the 2020–22 lava fountaining activity at Mt. Etna revealed by tilt deformation and volcanic tremor. *J. Volcanol. Geotherm. Res.* 449 (April), 108074. doi:10.1016/j.jvolgeores.2024.108074

Caricchi, L., Townsend, M., Rivalta, E., and Namiki, A. (2021). The build-up and triggers of volcanic eruptions. *Nat. Rev. Earth and Environ.* 2, 458–476. doi:10.1038/s43017-021-00174-8

Carleo, L., Currenti, G., and Bonaccorso, A. (2023). Clustering of eruptive events from high-precision strain signals recorded during the 2020–2022 lava fountains at the Etna volcano (Italy). *Nat. Hazards Earth Syst. Sci.* 23 (5), 1743–1754. doi:10.5194/nhess-23-1743-2023

Cashman, K. V., Sparks, R. S. J., and Blundy, J. D. (2017). Vertically extensive and unstable magmatic systems: a unified view of igneous processes. *Science* 355, eaag3055. doi:10.1126/science.aag3055

Chaussard, E., Amelung, F., and Aoki, Y. (2013). Characterization of open and closed volcanic systems in Indonesia and Mexico using InSAR time series. *J. Geophys. Res. Solid Earth* 118, 3957–3969. doi:10.1002/jgrb.50288

Colucci, S., and Papale, P. (2021). Deep magma transport control on the size and evolution of explosive volcanic eruptions. *Front. Earth Sci.* 9, 681083. doi:10.3389/feart.2021.681083

Cooper, G. F., Morgan, D. J., and Wilson, C. J. N. (2017). Rapid assembly and rejuvenation of a large silicic magmatic system: insights from mineral diffusive profiles in the Kidnappers and Rocky Hill deposits, New Zealand. *Earth Planet. Sci. Lett.* 473, 1–13. doi:10.1016/j.epsl.2017.05.036

Coppola, D., Laiolo, M., Massimetti, F., and Cigolini, C. (2019). Monitoring endogenous growth of open-vent volcanoes by balancing thermal and SO2 emissions data derived from space. *Sci. Rep.* 9, 9394. doi:10.1038/s41598-019-45753-4

Currenti, G., and Bonaccorso, A. (2019). Cyclic magma recharge pulses detected by high-precision strainmeter data: the case of 2017 inter-eruptive activity at Etna volcano. *Sci. Rep.* 9 (1), 7553–7557. doi:10.1038/s41598-019-44066-w

Del Negro, C., Currenti, G., and Scandura, D. (2009). Temperature-dependent viscoelastic modeling of ground deformation: application to Etna volcano during the 1993–1997 inflation period. *Phys. Earth Planet. Interiors* 172, 299–309. doi:10.1016/j.pepi.2008.10.019

Drooff, C., and Freymueller, J. T. (2021). New constraints on slip deficit on the Aleutian megathrust and inflation at Mt. Veniaminof, Alaska from repeat GPS measurements. *Geophys. Res. Lett.* 48, e2020GL091787. doi:10.1029/2020GL091787

Dzurisin, D. (2003). A comprehensive approach to monitoring volcano deformation as a window on the eruption cycle. *Rev. Geophys.* 41, 2001RG000107. doi:10.1029/2001RG000107

Dzurisin, D. (2007). *Volcano deformation: geodetic monitoring techniques*. Berlin: Springer. doi:10.1007/978-3-540-49302-0

Edmonds, M. (2021). "Geochemical monitoring of volcanoes and the mitigation of volcanic gas hazards," in *Forecasting and planning for volcanic hazards, risks, and disasters* (Elsevier), 117–151. doi:10.1016/B978-0-12-818082-2.00004-4

Fournier, T., and Freymueller, J. (2008). Inflation detected at Mount Veniaminof, Alaska, with campaign GPS. *Geophys. Res. Lett.* 35, 2008GL035503. doi:10.1029/2008GL035503

Ferretti, A., Prati, C., and Rocca, F. (2000). Nonlinear subsidence rate estimation using permanent scatterers in differential SAR interferometry. *IEEE. Transact. Geosci. Remo. Sensi.* 38 (5), 2202–2212.

Fournier, T. J., Pritchard, M. E., and Riddick, S. N. (2010). Duration, magnitude, and frequency of subaerial volcano deformation events: new results from Latin America using InSAR and a global synthesis. *Geochem. Geophys. Geosystems* 11, 2009GC002558. doi:10.1029/2009GC002558

Global Volcanism Program (2021). "Report on Veniaminof (United States)," in *Weekly volcanic activity report, 7–13 July 2021*. Editor Sennert, S. (Washington, DC, United States: Smithsonian Institution and US Geological Survey).

Gong, W., Meyer, F. J., Lee, C.-W., Lu, Z., and Freymueller, J. (2015). Measurement and interpretation of subtle deformation signals at Unimak Island from 2003 to 2010 using weather model-assisted time series InSAR. *J. Geophys. Res. Solid Earth* 120, 1175–1194. doi:10.1002/2014JB011384

Grapenthin, R., Freymueller, J. T., and Serovetnikov, S. S. (2013). Surface deformation of Bezymianny Volcano, Kamchatka, recorded by GPS: the eruptions from 2005 to 2010 and long-term, long-wavelength subsidence. *J. Volcanol. Geotherm. Res.* 263, 58–74. doi:10.1016/j.jvolgeores.2012.11.012

Gregg, P. M., De Silva, S. L., Grosfils, E. B., and Parmigiani, J. P. (2012). Catastrophic caldera-forming eruptions: thermomechanics and implications for eruption triggering and maximum caldera dimensions on Earth. *J. Volcanol. Geotherm. Res.* 241–242, 1–12. doi:10.1016/j.jvolgeores.2012.06.009

Gregg, P. M., Le Mével, H., Zhan, Y., Dufek, J., Geist, D., and Chadwick, W. W. (2018). Stress triggering of the 2005 eruption of sierra negra volcano, galápagos. *Geophys. Res. Lett.* 45. doi:10.1029/2018GL080393

Grosfils, E. B., McGovern, P. J., Gregg, P. M., Galgana, G. A., Hurwitz, D. M., Long, S. M., et al. (2015). Elastic models of magma reservoir mechanics: a key tool for investigating planetary volcanism. *Spec. Publ.* 401, 239–267. doi:10.1144/SP401.2

Gualda, G. A. R., Pamukcu, A. S., Ghiorso, M. S., Anderson, A. T., Sutton, S. R., and Rivers, M. L. (2012). Timescales of quartz crystallization and the longevity of the bishop giant magma body. *PLoS ONE* 7, e37492. doi:10.1371/journal.pone.0037492

Hanssen, R. F. (2001). "Radar system theory and interferometric processing," in *Radar Interferometry: data interpretation and error analysis* (Netherlands: Springer), 9–60. doi:10.1007/0-306-47633-9_2

Hickey, J., Gottsmann, J., and Del Potro, R. (2013). The large-scale surface uplift in the Altiplano-Puna region of Bolivia: a parametric study of source characteristics and crustal rheology using finite element analysis. *Geochem. Geophys. Geosystems* 14, 540–555. doi:10.1002/ggge.20057

Hooper, A., Zebker, H., Segall, P., and Kampes, B. (2004). A new method for measuring deformation on volcanoes and other natural terrains using InSAR persistent scatterers. *Geophys. Res. Lett.* 31, L23611. doi:10.1029/2004GL021737

Hooper, A. (2006). Persistent scatterer radar interferometry for crustal deformation studies and modeling of volcano deformation. PhD thesis. Stanford (California): Stanford University.

Hooper, A., Segall, P., and Zebker, H. A. (2007). Persistent scatterer radar interferometry for crustal deformation studies and modeling of volcanic deformation. *J. Geophys. Res. Solid. Earth.* 112, B07407. doi:10.1029/2006JB004714

Hooper, A., Segall, P., and Zebker, H. A. (2007). Persistent scatterer interferometric synthetic aperture radar for crustal deformation analysis, with application to Volcán Alcedo, Galápagos. *J. Geophys. Res. Solid. Earth.* 112, B07407. doi:10.1029/2006JB004763

Hooper, A. (2008). A multi-temporal InSAR method incorporating both persistent scatterer and small baseline approaches. *Geophys Res. Lett.* 35, L16302. doi:10.1029/2008GL034654

Jellinek, A. M., and DePaolo, D. J. (2003). A model for the origin of large silicic magma chambers: precursors of caldera-forming eruptions. *Bull. Volcanol.* 65, 363–381. doi:10.1007/s00445-003-0277-y

Johnson, J. B., Watson, L. M., Palma, J. L., Dunham, E. M., and Anderson, J. F. (2018). Forecasting the eruption of an open-vent volcano using resonant infrasound tones. *Geophys. Res. Lett.* 45, 2213–2220. doi:10.1002/2017GL076506

Jousset, P., Currenti, G., Murphy, S., Eibl, E. P. S., Caudron, C., Retailleau, L., et al. (2025). "Fiber optic sensing for volcano monitoring and imaging volcanic processes," in *Modern Volcano monitoring* (Springer).

Karakas, O., Degruyter, W., Bachmann, O., and Dufek, J. (2017). Lifetime and size of shallow magma bodies controlled by crustal-scale magmatism. *Nat. Geosci.* 10, 446–450. doi:10.1038/ngeo2959

Le Mével, H., Gregg, P. M., and Feigl, K. L. (2016). Magma injection into a long-lived reservoir to explain geodetically measured uplift: Application to the 2007–2014 unrest episode at Laguna del Maule volcanic field, Chile. *J. Geophys. Res. Solid Earth* 121, 6092–6108. doi:10.1002/2016JB013066

Linde, A. T., and Sacks, S. I. (1995). "Continuous monitoring of volcanoes with borehole strainmeters,". *Mauna loa revealed: structure, composition, hystory, and hazards*. Editors J. M. Rhodes, and J. P. Lockwood (Washington DC: American Geophysical Union), 171, 171–185. doi:10.1029/gm092p0171

Loewen, M. W., Dietterich, H. R., Graham, N., and Izbekov, P. (2021). Evolution in eruptive style of the 2018 eruption of Veniaminof volcano, Alaska, reflected in groundmass textures and remote sensing. *Bull. Volcanol.* 83, 72. doi:10.1007/s00445-021-01489-6

Lu, Z., and Dzurisin, D. (2014). *InSAR imaging of aleutian volcanoes: monitoring a volcanic arc from space*. Springer Berlin Heidelberg. doi:10.1007/978-3-642-00348-6

Lu, Z., Wicks, C., Dzurisin, D., Thatcher, W., Freymueller, J. T., McNutt, S. R., et al. (2000). Aseismic inflation of Westdahl Volcano, Alaska, revealed by satellite radar interferometry. *Geophys. Res. Lett.* 27, 1567–1570. doi:10.1029/1999 GL011283

Lyons, J., Rose, B., and Escobar, R. (2011). Volcanic hazards and remote sensing in Pacific Latin America. *EoS Trans.* 92, 196. doi:10.1029/2011EO230007

Malfante, M., Dalla Mura, M., Metaxian, J.-P., Mars, J. I., Macedo, O., and Inza, A. (2018). Machine learning for volcano-seismic signals: challenges and perspectives. *IEEE Signal Process. Mag.* 35, 20–30. doi:10.1109/MSP.2017.2779166

Malone, S. D., Boyko, C., and Weaver, C. S. (1983). Seismic precursors to the Mount St. Helens eruptions in 1981 and 1982. *Science* 221, 1376–1378. doi:10.1126/science.221.4618.1376

Manley, G. F., Mather, T. A., Pyle, D. M., Clifton, D. A., Rodgers, M., Thompson, G., et al. (2021). Machine learning approaches to identifying changes in eruptive state using multi-parameter datasets from the 2006 eruption of Augustine Volcano, Alaska. *J. Geophys. Res. Solid Earth* 126, e2021JB022323. doi:10.1029/2021JB022323

Marzocchi, W., and Bebbington, M. S. (2012). Probabilistic eruption forecasting at short and long time scales. *Bull. Volcanol.* 74, 1777–1805. doi:10.1007/s00445-012-0633-x

Matoza, R. S., and Fee, D. (2018). The inaudible rumble of volcanic eruptions. *Acoust. Today* 14 (1).

Miller, T. P., McGimsey, R. G., Richter, D. H., Riehle, J. R., Nye, C. J., Yount, M. E., et al. (1998). Catalog of the historically active volcanoes of Alaska (No. 98–582). *Open-File Rep*. doi:10.3133/ofr98582

Miller, T. P., and Smith, R. L. (1987). Late Quaternary caldera-forming eruptions in the eastern Aleutian arc, Alaska. *Geology* 15, 434–438. doi:10.1130/0091-7613(1987)15<434:LQCEIT>2.0.CO;2

Mittal, T., and Richards, M. A. (2019). Volatile degassing from magma chambers as a control on volcanic eruptions. *J. Geophys. Res. Solid Earth* 124, 7869–7901. doi:10.1029/2018JB016983

Moran, S. C., Kwoun, O., Masterlark, T., and Lu, Z. (2006). On the absence of InSAR-detected volcano deformation spanning the 1995–1996 and 1999 eruptions of Shishaldin Volcano, Alaska. *J. Volcanol. Geotherm. Res.* 150, 119–131. doi:10.1016/j.jvolgeores.2005.07.013

Newman, A. V., Dixon, T. H., Ofoegbu, G. I., and Dixon, J. E. (2001). Geodetic and seismic constraints on recent activity at Long Valley Caldera, California: evidence for viscoelastic rheology. *J. Volcanol. Geotherm. Res.* 105, 183–206. doi:10.1016/S0377-0273(00)00255-9

Orr, T. R., Neal, C. A., and Power, J. A. (2024). *Observations of the 2021 eruption of Mount Veniaminof.* Alaska: U.S. Geological Survey Scientific Investigations Report, 2024–5014. doi:10.3133/sir20245014

Phillipson, G., Sobradelo, R., and Gottsmann, J. (2013). Global volcanic unrest in the 21st century: an analysis of the first decade. *J. Volcanol. Geotherm. Res.* 264, 183–196. doi:10.1016/j.jvolgeores.2013.08.004

Poland, M. P., and Anderson, K. R. (2020). Partly cloudy with a chance of lava flows: forecasting volcanic eruptions in the twenty-first century. *J. Geophys. Res. Solid Earth* 125, e2018JB016974. doi:10.1029/2018JB016974

Power, J., Friberg, P. A., Haney, M. M., Parker, T., Stihler, S. D., and Dixon, J. P. (2019). *A unified catalog of earthquake hypocenters and magnitudes at volcanoes in Alaska—1989 to 2018 (No. 2019–5037)*. Scientific Investigations Report, U.S. Geological Survey. doi:10.3133/sir20195037

Power, J. A., Haney, M. M., Botnick, S. M., Dixon, J. P., Fee, D., Kaufman, A. M., et al. (2020). Goals and development of the Alaska Volcano Observatory seismic network and application to forecasting and detecting volcanic eruptions. *Seismol. Res. Lett.* 91, 647–659. doi:10.1785/0220190216

Power, J. A., Stihler, S. D., White, R. A., and Moran, S. C. (2004). Observations of deep long-period (DLP) seismic events beneath Aleutian arc volcanoes; 1989–2002. *J. Volcanol. Geotherm. Res.* 138, 243–266. doi:10.1016/j.jvolgeores.2004.07.005

Rasmussen, D. J., Plank, T. A., Roman, D. C., Power, J. A., Bodnar, R. J., and Hauri, E. H. (2018). When does eruption run-up begin? Multidisciplinary insight from the 1999 eruption of Shishaldin volcano. *Earth Planet. Sci. Lett.* 486, 1–14. doi:10.1016/j.epsl.2018.01.001

Reichstein, M., Camps-Valls, G., Stevens, B., Jung, M., Denzler, J., Carvalhais, N., and Prabhat, F.(2019). Deep learning and process understanding for data-driven Earth system science. *Nature* 566, 195–204. doi:10.1038/s41586-019-0912-1

Roman, D. C., and Cashman, K. V. (2018). Top-down precursory volcanic seismicity: implications for 'stealth' magma ascent and long-term eruption forecasting. *Front. Earth Sci.* 6, 124. doi:10.3389/feart.2018.00124

Rose, W. I., Palma, J. L., Delgado Granados, H., and Varley, N. (2013). "Open-vent volcanism and related hazards: overview," in *Understanding open-vent volcanism and related hazards*. Editors W. I. Rose, J. L. Palma, H. Delgado Granados, and N. Varley (Boulder, CO, United States: Geological Society of America). doi:10.1130/2013.249800 498, vii–Xiii.

Segall, P. (2013). Volcano deformation and eruption forecasting. *Spec. Publ.* 380, 85–106. doi:10.1144/SP380.4

Sparks, R. S. J., Biggs, J., and Neuberg, J. W. (2012). Monitoring volcanoes. *Science* 335, 1310–1311. doi:10.1126/science.1219485

Soosalu, H., Einarsson, P., and Þorbjarnardóttir, B. S. (2005). Seismic activity related to the 2000 eruption of the Hekla volcano, Iceland. *Bull. Volcanol.* 38, 21–36. doi:10.1007/s00445-005-0417-7

Swanson, D. A., Casadevall, T. J., Dzurisin, D., Malone, S. D., Newhall, C. G., and Weaver, C. S. (1983). Predicting eruptions at Mount St. Helens, june 1980 through december 1982. *Science* 221, 1369–1376. doi:10.1126/science.221.4618.1369

Turner, S., and Costa, F. (2007). Measuring timescales of magmatic evolution. *Elements* 3, 267–272. doi:10.2113/gselements.3.4.267

Voight, B., Hoblitt, R. P., Clarke, A. B., Lockhart, A. B., Miller, A. D., Lynch, L., et al. (1998). Remarkable cyclic ground deformation monitored in real-time on Montserrat, and its use in eruption forecasting. *Geophys. Res. Lett.* 25, 3405–3408. doi:10.1029/98GL01160

Voight, B., Sparks, R. S. J., Miller, A. D., Stewart, R. C., Hoblitt, R. P., Clarke, A., et al. (1999). Magma flow instability and cyclic activity at soufriere hills volcano, Montserrat, British west indies. *Science* 283, 1138–1142. doi:10.1126/science.283.5405.1138

Wallace, K. L., Cameron, C. E., Waythomas, C. F., and Perreault, J. M. (2020). *Major-oxide and trace-element geochemical data from the tephra collected on Veniaminof volcano, Alaska (No. RDF 2020-17)*. Fairbanks, AK, United States: Alaska Division of Geological and Geophysical Surveys. doi:10.14509/30578

Waythomas, C. F. (2021). Simultaneous effusive and explosive cinder cone eruptions at Veniaminof Volcano, Alaska. *Volcanica* 4, 295–307. doi:10.30909/vol.04.02.295307

Waythomas, C. F., Cameron, C. E., and Miller, T. P. (2022). *Eruptive history and hazards of Mount Veniaminof, Alaska*. U.S. Geological Survey Scientific Investigations Report, 2022–5075. doi:10.3133/sir20225075

Wilkes, T. C., Pering, T. D., Aguilera, F., Layana, S., Nadeau, P., Kern, C., et al. (2023). A new permanent, low-cost, low-power SO2 camera for continuous measurement of volcanic emissions. *Front. Earth Sci.* 11, 1088992. doi:10.3389/feart.2023.1088992

Zhan, Y., and Gregg, P. M. (2019). How accurately can we model magma reservoir failure with uncertainties in host rock rheology? *J. Geophys. Res. Solid Earth* 124, 8030–8042. doi:10.1029/2019JB018178

Zhu, W., and Beroza, G. C. (2018). PhaseNet: a deep-neural-network-based seismic arrival time picking method. *Geophys. J. Int*. doi:10.1093/gji/ggy423